Tungstate-Based Inorganic−Organic Hybrid Nanobelts/Nanotubes with Lamellar Mesostructures: Synthesis, Characterization, and Formation Mechanism

Deliang Chen and Yoshiyuki Sugahara*

Department of Applied Chemistry, School of Science and Engineering, Waseda University, Shinjuku-ku, Tokyo 169-8555, Japan

Received August 29, 2006. Revised Manuscript Received December 26, 2006

The formation process of novel tungstate-based inorganic−organic hybrid nanobelts/nanotubes with lamellar mesostructures has been investigated, with an emphasis on monitoring the morphological and microstructural changes of the products during the reactions of $H_2W_2O_7{\cdot}xH_2O$ ($x = 3.49$) with *n*-alkylamines ($C_mH_{2m+1}NH_2$, $4 \leq m \leq 14$) in a system of heptane/*n*-alkylamine/$H_2W_2O_7{\cdot}xH_2O$ (*n*-alkylamine:$H_2W_2O_7{\cdot}xH_2O$ molar ratio of about 30) under ambient conditions. The results indicate that normal intercalation occurrs in the early stage to form intercalation compounds with double-octahedral W−O layers, which are then dissolved in the highly alkaline aqueous solutions confined in the reverse-micelle-like media, where the dissolved species recrystallize to form hybrid nanobelts/nanotubes with single-octahedral W−O layers. Both the intercalation compounds obtained after a short reaction time (e.g., 30 min) and the hybrid nanobelts/nanotubers formed after a long reaction time (e.g., 5 days) possess a bilayered arrangement of *n*-alkyl chains, but their tilt angle in the intercalation compounds (42°) is much smaller than that in the hybrid nanobelts/nanotubes (71°). The interlayer water released from $H_2W_2O_7{\cdot}xH_2O$ upon intercalation of *n*-alkylamine reacts with excess *n*-alkylamine molecules to form highly alkaline aqueous solutions, which have vital effects on the subsequent dissolution of the double-octahedral W−O layers to be single-octahedral layers. In addition, the high molar *n*-alkylamine:$H_2W_2O_7{\cdot}xH_2O$ ratios (e.g., 30) are necessary to form tungstate-based inorganic−organic nanobelts/nanotubes, and the nonpolar solvents not only facilitate the reactions between *n*-alkylamines and $H_2W_2O_7{\cdot}xH_2O$ but also favor the formation of belt/tubelike morphology.

Introduction

The Chimie Douce approach is a rational design strategy with respect to novel materials and structures.[1] On the basis of this strategy, a variety of metastable solid materials have been synthesized.[2] Inserting guest species into a layered compound is an effective route to lamellarly meso-/nanoporous hybrid nanomaterials.[3−7] Among these, the mesostructured inorganic−organic hybrids derived from layered compounds on the basis of intercalation chemistry (so-called "intercalation compounds") have attracted constant interest because of the significance for inorganic chemistry[8−13] and technological applications.[14−18]

The stability of the inorganic layers is an important factor in intercalation chemistry, because it is directly related to the reaction mechanism. The inorganic layers in inorganic−organic hybrids are usually thought to be derived from the corresponding host layered compounds without any decomposition or modification.[11,19−23] In fact, the modification of inorganic layers often occurs in a few cases, typical examples of which are alkyltrimethylammonium (C_nTMA)−kanemite complex precursors for KSW and FSW mesoporous materials, the inorganic frameworks of which have been thought to derive from the curving silicate layers.[24−26] There are, on

* Corresponding author. E-mail: ys6546@waseda.jp.

(1) Sanchez, C.; Soler-Illia, G. J. A. A.; Ribot, F.; Lalot, T.; Mayer, C. R.; Cabuil, V. *Chem. Mater.* **2001**, *13*, 3061.
(2) (a) Xiang, X.-D.; McKernan, S.; Vareka, W. A.; Zettl, A.; Corkill, J. L.; Barbee, T. W.; Cohen, M. L. *Nature* **1990**, *348*, 145. (b) Zhou, O.; Fleming, R. M; Murphy, D. W.; Rosseinsky, M. J.; Ramirez, A. P.; Dover, R. B.; Haddon, R. C. Nature **1993**, *362*, 433. (c) Mallouk, T. E.; Gavin, J. A. *Acc. Chem. Res.* **1998**, *31*, 209. (d) Shan, Y.; Huang, R. H.; Huang, S. D. *Angew. Chem., Int. Ed.* **1999**, *38*, 1751. (e) Takada, K.; Sakurai, H.; Takayama-Muromachi, E.; Izumi, F.; Dilanian, R. A.; Sasaki, T. *Nature* **2003**, *422*, 53.
(3) *Inorganic Materials*, 2nd ed.; Bruce, D. W., O'Hare, D., Eds.; John Wiley & Sons: New York, 1999.
(4) *Handbook of Layered Materials*; Auerbach, S. M., Carrado, K. A., Dutta, P. K., Eds.; Marcel Dekker: New York, 2004.
(5) *Intercalation Chemistry*; Whittingham, M. S., Jacobson, A. J., Eds.; Academic Press: New York, 1982.
(6) Ohtsuka, K. *Chem. Mater.* **1997**, *9*, 2039.
(7) Triantafillidis, C. S.; LeBaron, P. C.; Pinnavaia, T. J. *Chem. Mater.* **2002**, *14*, 4088.
(8) Shpeizer, B. G.; Ouyang, X.; Heising, J. M.; Clearfield, A. *Chem. Mater.* **2001**, *13*, 2288.
(9) (a) Lagaly, G.; Beneke, K. *Colloid Polym. Sci.* **1991**, *269*, 1198. (b) Lagaly, G. *Solid State Ionics* **1986**, *22*, 43. (c) Lagaly, G. *Angew. Chem., Int. Ed.* **1976**, *15*, 575.
(10) Ogawa, M.; Kuroda, K. *Bull. Chem. Soc. Jpn.* **1997**, *70*, 2593.
(11) (a) Alberti, G.; Marmottini, F.; Cavalaglio, S.; Severi, D. *Langmuir* **2000**, *16*, 4165. (b) Guliants, V. V.; Benziger, J. B.; Sundaresan, S. *Chem. Mater.* **1994**, *6*, 353.
(12) Breu, J.; Catlow, C. R. A. *Inorg. Chem.* **1995**, *34*, 4504.
(13) Wang, Q.; Gao, Q.; Shi, J. *J. Am. Chem. Soc.* **2004**, *126*, 14346.
(14) (a) Johnson, J. W.; Jacobson, A. J.; Butler, W. M.; Rosenthal, S. E.; Brody, J. F.; Lewandowski, J. T. *J. Am. Chem. Soc.* **1989**, *111*, 381. (b) Ogawa, M.; Okutomo, S.; Kuroda, K. *J. Am. Chem. Soc.* **1998**, *120*, 7361.
(15) Zhong, Z.; Ding, W.; Hou, W.; Chen, Y.; Chen, X.; Zhu, Y.; Min, N. *Chem. Mater.* **2001**, *13*, 538.
(16) (a) Kanatzidis, M. G.; Sutorik, A. C. *Prog. Inorg. Chem.* **1995**, *43*, 151. (b) Kanatzidis, M. G.; Wu, C. G.; Marcy, H. O.; Kannewurf, C. R. *J. Am. Chem. Soc.* **1989**, *111*, 4139.
(17) Yamagishi, A. *J. Phys. Chem.* **1982**, *86*, 2472.

10.1021/cm062039u CCC: $37.00
Published on Web 03/07/2007

the other hand, also some inorganic layers that undergo a certain decomposition during the reaction process.[27] It is therefore not always appropriate to assume that the inorganic layers remain intact during the reactions, especially in the case of those exhibiting a tendency to dissolve in guest solutions. Monitoring the dynamic changes of the morphology and microstructure of the hybrids will be an effective approach for reaching a proper understanding of intercalation chemistry.

Tungsten-oxide-based materials, including the inorganic−organic hybrids,[28−30] have attracted increasing interest because of their unique properties and corresponding applications in optics, electronics, and catalysis.[31−36] Tungsten oxide hydrates include H_2WO_4 (or $H_2WO_4{\cdot}xH_2O$) with single-octahedral W−O layers and $H_2W_2O_7{\cdot}xH_2O$ with double-octahedral W−O layers, both of which can be used as the host compounds for intercalation.[37−39] $H_2W_2O_7{\cdot}xH_2O$ can be derived by selectively leaching Bi_2O_2 layers from the cation-deficient Aurivillius phase of $Bi_2W_2O_9$.[38,39] Johnson et al. reported a layered inorganic−organic hybrid of $WO_3C_5H_5N$ achieved by heating H_2WO_4 with excess pyridine in the presence of molecular sieves at 423 K.[37a] Mallouk et al. reported the exfoliation of $H_2W_2O_7$ into $TBA_xH_{2-x}W_2O_7$ nanosheets in a quaternary ammonium hydroxide (TBA^+OH^-) aqueous solution.[39] Our recent report also indicated the possible intercalation of *n*-alkylamines into $H_2W_2O_7{\cdot}xH_2O$.[38] It is well-known, on the other hand, that tungsten oxides and their hydrates can easily be dissolved in alkaline aqueous solutions.[40,41] As concerns the intercalation chemistry of layered tungstates, there are still a multitude of issues which are not fully understood.

We report here an investigation of the reaction between layered $H_2W_2O_7{\cdot}xH_2O$ and *n*-alkylamines, with an emphasis placed on the dynamical monitoring of the changes of the morphology and microstructure of the products in various reaction stages. *n*-Alkylamines with various *n*-alkyl chain lengths are excellent model guest molecules for intercalation research.[9,10] The double-octahedral W−O layers in layered $H_2W_2O_7{\cdot}xH_2O$ can be used as identifiers, which can give useful information concerning the stability of the inorganic layers. The morphological changes and microstructural development of the products in various reaction stages, the stability of the inorganic W−O layers, the effects of *n*-alkylamine:$H_2W_2O_7{\cdot}xH_2O$ ratios and solvent types on the product morphology and microstructure, and the related mechanisms are addressed in some detail in the present study.

Experimental Section

Synthesis. Typically, a stoichiometric mixture of Bi_2O_3 (99.99%) and WO_3 (99.9%) was calcined at 1073 K for 48 h with intermittent grinding to synthesize $Bi_2W_2O_9$. The calculated cell parameters (a = 0.542(2) nm, b = 0.541(2) nm, c = 2.36(1) nm) were close to the literature values (a = 0.5440(1) nm, b = 0.5413(1) nm, c = 2.3740(5) nm),[42] which indicated a successful synthesis of the pure $Bi_2W_2O_9$ phase with an orthorhombic crystal system ($Pna2_1$).[42] Selective leaching of Bi_2O_2 layers from $Bi_2W_2O_9$ by hydrochloric acid treatment resulted in the formation of its protonated phase, $H_2W_2O_7{\cdot}xH_2O$, according to the previously reported process with some modification.[38] Typically, as-obtained $Bi_2W_2O_9$ (about 10 g) was dispersed in hydrochloric acid (1 L, about 6 M) and stirred constantly for a week at 298 K. After centrifugation and washing, the yellow solid obtained was air-dried at 298 K for 3 days. The calculated cell parameters based on its XRD pattern were a = 0.521(7) nm, b = 0.518(7) nm, and c = 2.23(4) nm, consistent with the reported values (a = 0.524(1) nm, b = 0.513(1) nm, c = 2.21(1) nm).[38] TG analysis suggested that the amount of interlayer water in the air-dried $H_2W_2O_7{\cdot}xH_2O$ typically corresponded to x = 3.49. It is worth noting that the amount of interlayer water depended completely on the drying conditions. The as-obtained $H_2W_2O_7{\cdot}xH_2O$ was used as the host compound for the following reactions with *n*-alkylamines.

The reactions between $H_2W_2O_7{\cdot}xH_2O$ and *n*-alkylamines were carried out at room temperature under an ambient atmosphere. Essentially the same procedure was applied for *n*-alkylamines with various alkyl chain lengths ($C_mH_{2m+1}NH_2$, $4 \le m \le 14$). The molar ratios of *n*-alkylamine to $H_2W_2O_7{\cdot}xH_2O$ were about 30, and the volume ratios of heptane to *n*-alkylamine were maintained at about 2. Typically, about 0.3 g of the air-dried $H_2W_2O_7{\cdot}xH_2O$ was

(18) Ogawa, M.; Kuroda, K. *Chem. Rev.* **1995**, *95*, 399.
(19) (a) Yamamoto, N.; Okuhara, T.; Nakato, T. *J. Mater. Chem.* **2001**, *7*, 1858. (b) Beneš, L.; Melánová, K.; Zima, V.; Patrono, P.; Galli, P. *Eur. J. Inorg. Chem.* **2003**, *8*, 1577. (c) Thoma, S. G.; Bonhomme, F.; Cygan, R. T. *Chem. Mater.* **2004**, *16*, 2068.
(20) (a) Kinomura N.; Kumada, N. *Solid State Ionics* **1992**, *51*, 1. (b) Kinomura, N.; Amano, S.; Kumada, N. *Solid State Ionics* **1990**, *37*, 317. (c) Bhat, V.; Gopalakrishnan, J. *Solid State Ionics* **1988**, *26*, 25. (d) Peng, L.; Yu, J.; Li, J.; Li, Y.; Xu, R. *Chem. Mater.* **2005**, *17*, 2101.
(21) Yang, J. H.; Han, Y. S.; Choy, J. H.; Tateyama, H. *J. Mater. Chem.* **2001**, *11*, 1305.
(22) Wortham, E.; Bonnet, B.; Jones, D. J.; Roziére, J.; Burns, G. R. *J. Mater. Chem.* **2004**, *1*, 121.
(23) Shukoor, M. I.; Therese, H. A.; Gorgishvili, L.; Glasser, G.; Kolb, U.; Tremel, W. *Chem. Mater.* **2006**, *18*, 2144.
(24) Yanagisawa, T.; Shimizu, T.; Kuroda, K.; Kato, C. *Bull. Chem. Soc. Jpn.* **1990**, *63*, 988.
(25) (a) Inagaki, S.; Fukushima, Y.; Kuroda, K. *J. Chem. Soc., Chem. Commun.* **1993**, 680. (b) Kuroda, K. *J. Porous Mater.* **1996**, *3*, 107.
(26) Kimura, T.; Kamata, T.; Fuziwara, M.; Takano, Y.; Kaneda, M.; Sakamoto, Y.; Terasaki, O.; Sugahara, Y.; Kuroda, K. *Angew. Chem., Int. Ed.* **2000**, *39*, 3855.
(27) (a) Hibino, T.; Tsunashima, A. *Chem. Mater.* **1997**, *9*, 2082. (b) Gardolinski, J. E. F. C.; Lagaly, G.; Czank, M. *Clay Miner.* **2004**, *39*, 391.
(28) Ayyappan, S.; Subbanna, G. N.; Rao, C. N. R. *Chem.—Eur. J.* **1995**, *1*, 165.
(29) (a) Yan, B.; Xu, Y.; Goh, N. K.; Chia, L. S. *Chem. Commun.* **2000**, 2169. (b) Yan, B.; Xu, Y.; Goh, N. K.; Chia, L. S. *Inorg. Chem. Commun.* **2000**, *3*, 379.
(30) (a) Chong, S. V.; Ingham, B.; Tallon, J. L. *Curr. Appl. Phys.* **2004**, *4*, 197. (b) Ingham, B.; Chong, S. V.; Tallon, J. L. *Curr. Appl. Phys.* **2004**, *4*, 202. (c) Ingham, B.; Chong, S. V.; Tallon, J. L. *J. Phys. Chem. B* **2005**, *109*, 4936.
(31) Bange, K.; Gambke, T. *Adv. Mater.* **1990**, *2*, 10.
(32) Feng, M.; Pan, A. L.; Zhang, H. R.; Li, Z. A.; Liu, F.; Liu, H. W.; Shi, D. X.; Zou, B. S.; Gao, H. J. *Appl. Phys. Lett.* **2005**, *86*, 141901.
(33) Wei, X. L.; Shen, P. K. *Electrochem. Commun.* **2006**, *8*, 293.
(34) Wachs, I. E.; Kim, T.; Ross, E. I. *Catal. Today* **2006**, *116*, 162.
(35) Baeck, S. H.; Choi, K. S.; Jaramillo, T. F.; Stucky, G. D.; McFarland, E. W. *Adv. Mater.* **2003**, *15*, 1269.
(36) (a) Polleux, J.; Pinna, N.; Antonietti, M.; Niederberger, M. *J. Am. Chem. Soc.* **2005**, *127*, 15595. (b) Polleux, J.; Gurlo, A.; Barsan, N.; Weimar, U; Antonietti, M.; Niederberger, M. *Angew. Chem., Int. Ed.* **2006**, *45*, 261.
(37) (a) Johnson, J. W.; Jacobson, A. J.; Rich, S. M.; Brody, J. F. *J. Am. Chem. Soc.* **1981**, *103*, 5246. (b) Chemseddine, A.; Babonneau, F.; Livage, J. *J. Non-Cryst. Solids* **1987**, *91*, 271.
(38) Kudo, M.; Ohkawa, H.; Sugimoto, W.; Kumada, N.; Liu, Z.; Terasaki, O.; Sugahara, Y. *Inorg. Chem.* **2003**, *42*, 4479.
(39) Schaak, R. E.; Mallouk, T. E. *Chem. Commun.* **2002**, 706.
(40) Martins, J. I.; Delmas, F.; Casquinha, H.; Costa, S. *Hydrometallurgy* **2002**, *67*, 117.
(41) De Benneville, J. S. *J. Am. Chem. Soc.* **1897**, *19*, 377.
(42) Champarnaut-Mesjard, J. C; Frit, B.; Watanabe, A. *J. Mater. Chem.* **1999**, *9*, 1319.

dispersed in the mixtures of heptane and *n*-alkylamine with magnetic stirring. After reacting for 30 min or 5 days, the products were collected from the suspensions by centrifugation and washed with ethanol. Other solvents, such as acetone, ethanol, 2-propanol, butanol, 1-octanol, tetrahydrofuran (THF), pentane, decane, 2,2,4-trimethylpentane, and cyclohexane, were also used as the solvents for the reactions between $H_2W_2O_7{\cdot}xH_2O$ and *n*-octylamine under the similar conditions. For the investigation of the morphological changes with reaction time, about 1.0 g of the air-dried $H_2W_2O_7{\cdot}xH_2O$ (about 2 mmol) was dispersed in the mixture of *n*-octylamine (10 mL, about 60 mmol) and heptane (20 mL). After various reaction times (from 0.5 h to several days), an appropriate amount of suspension was removed from the same suspension pot, followed by centrifugation and washing. The reaction with an *n*-octylamine-to-$H_2W_2O_7{\cdot}xH_2O$ molar ratio of 2 was also conducted as follows: about 0.3 g of $H_2W_2O_7{\cdot}xH_2O$ was dispersed in 15 mL of heptane and stirred constantly for 5 days. All the products obtained were dried at room temperature under reduced pressure for 2−3 days.

Characterization. X-ray diffraction (XRD) measurements were performed on a Rigaku RINT-2500 diffractometer with Cu Kα radiation or on a MacScience M03X-HF[22] diffractometer with Mn-filtered Fe Kα radiation. Scanning electron microscopy (SEM) images were recorded with a JEOL JSM-5600 microscope at an accelerating voltage of 10 kV. Field-emission scanning electron microscopy (FE-SEM) images were obtained with a Hitachi S-4500S microscope with an accelerating voltage of 15 kV. Transmission electron microscopy (TEM) images and selected area electron diffraction (SAED) patterns were obtained with a JEOL JEM-100CX microscope with an accelerating voltage of 100 kV, or on a Hitachi H-8100A microscope with an accelerating voltage of 200 kV. For the preparation of TEM samples, the products were redispersed in ethanol and appropriate amounts of the suspensions were dropped on Cu grids. Thermogravimetry (TG) measurements were carried out on a Perkin-Elmer thermobalance TGA-7 with a heating rate of 10 K min^{-1} in an air flow. CHN analysis was performed with a Perkin-Elmer PE2400II instrument. Fourier-transform infrared (FT−IR) spectra were recorded on a Jasco FT−IR 460 Plus spectrophotometer using the KBr disk technique.

Results and Discussion

Reaction of $H_2W_2O_7{\cdot}xH_2O$ with *n*-Alkylamines. The XRD patterns of the products obtained from reactions between *n*-octylamine and $H_2W_2O_7{\cdot}xH_2O$ (30:1 in molarity) in heptane with various reaction periods (0.5−120 h) are shown in Figure 1. A new series of reflections occur in the low 2θ angle region for the product with a reaction time of 0.5 h, as shown in Figure 1b. At the same time, the reflections due to air-dried $H_2W_2O_7{\cdot}xH_2O$, as shown in Figure 1a, disappear.[38] The sharp reflections in the low 2θ range can be indexed to (00*l*) reflections from a highly ordered lamellar structure. The number of identifiable reflections is up to six, but their intensities are very low for the reflections with $l \geq 2$. With increases in reaction time, the intensities of the (00*l*) reflections become stronger. The interlayer distance of the product with a reaction time of 120 h is determined to be 2.59(1) nm according to its (00*l*) reflections, shown in Figure 1h.

The SEM images of the products obtained with various reaction periods are shown in Figure 2. As Figure 2a shows, the host compound of $H_2W_2O_7{\cdot}xH_2O$ takes on platelike shapes with distinct cleavage planes, and the particle sizes range from 5 to 20 μm. The product with a reaction time of

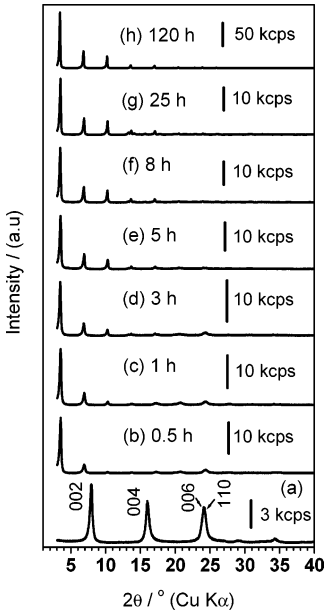

Figure 1. XRD patterns of the products accommodating *n*-octylamine obtained in a system of heptene/*n*-octylamine/$H_2W_2O_7{\cdot}xH_2O$ with various reaction times (*n*-octylamine:$H_2W_2O_7{\cdot}xH_2O$ molar ratio of 30): (a) 0 ($H_2W_2O_7{\cdot}xH_2O$), (b) 0.5, (c) 1, (d) 3, (e) 5, (f) 8, (g) 25, and (h) 120 h.

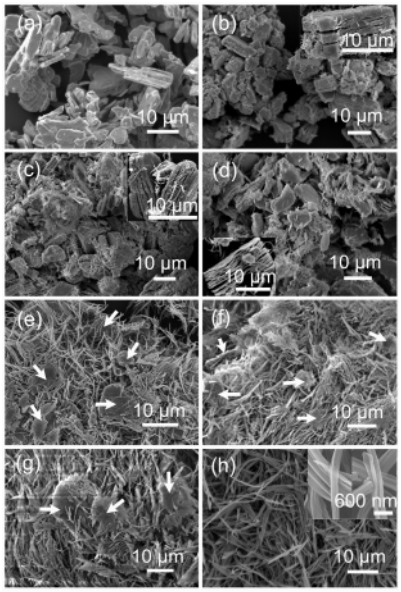

Figure 2. SEM images of the products accommodating *n*-octylamine after various reaction times (*n*-octylamine:$H_2W_2O_7{\cdot}xH_2O$ molar ratio of 30): (a) 0 ($H_2W_2O_7{\cdot}xH_2O$), (b) 0.5, (c) 1, (d) 3, (e) 5, (f) 8, (g) 25, and (h) 120 h (the inset of h is an FE-SEM image).

0.5 h (Figure 2b) shows parallel cracks, by which the particles are separated into plates with thicknesses of 1−2 μm. With longer reaction periods (e.g., 1−3 h), the products obtained exhibit thinner plates, with plate thicknesses of 200−800 nm, as shown in images c and d of Figure 2, and the platelike particles are the major morphology. After a reaction time of 5 h, a certain percentage of the plates has begun to be transformed into filamentous structures, as shown in Figure 2e. With the continuation of the reaction period to 8 and 25 h, more platelike particles have been transformed into filamentous structures, as shown in images f and g of Figure 2. For the products with reaction periods of 5−25 h, the platelike particles continue to coexist (indicated by arrows

Table 1. Summary of Mass Loss (M_L) between Room Temperature and 873 K, Data for CHN Analysis, and the Molar Ratio (R) of *n*-Octylamine Taken up to W of the Products as a Function of Reaction Time (t)

t (h)	M_L (mass %)	C (mass %)	H (mass %)	N (mass %)	R
0.5	21.8	17.68	3.64	2.66	0.563
1	23.7	18.39	3.78	2.73	0.592
3	25.4	19.02	4.03	2.81	0.623
5	36.7	25.52	5.16	3.72	0.973
8	41.3	30.85	6.37	4.51	1.27
25	48.1	35.19	7.31	5.10	1.63
120	52.9	42.48	8.57	6.16	2.16

in Figure 2) with the gradually increasing filamentous structures. The product obtained with a reaction time of 120 h takes on a uniform filamentous structure (Figure 2h). The FE-SEM image (upper right inset in Figure 2h) and TEM image (see the Supporting Information, Figure S1) indicate that the filamentous structures are nanobelts or nanotubes with apparent diameters of 200−700 nm and lengths of 5−20 μm. The thicknesses of the nanobelts and the nanotube walls are 20−50 nm.

The TG curves (see the Supporting Information, Figure S2) indicate that the mass-loss-curve profiles of the products with various reaction times are similar. The mass loss between room temperature and 873 K increases from 21.8% for the product with a reaction time of 0.5 h to 52.9% for the product with a reaction time of 120 h, as summarized in Table 1. The CHN data are also listed in Table 1. The calculated ratios of C:H:N in moles are (7.8−8.0):(19.2−20.1):1, results very close to the composition (8:19:1 for C:H:N) of *n*-octylamine.

The typical FT−IR spectra of the products (see the Supporting Information, Figure S3) show an intense absorption band at around 900 cm^{-1}, which is assignable to the stretching mode of terminal W═O.[30c] The bands located at around 580−860 and 418−435 cm^{-1} can be assigned to the stretching and bending modes of the bridging oxygen atoms (O−W−O), respectively.[30c] The sharp bands at 3100−3300 cm^{-1} can be assigned to the stretching vibration of the N−H groups.[30c,43] Bands due to both the scissoring mode of the $-NH_2$ groups and the bending mode of the $-NH_3^+$ groups appear between 1630 and 1580 cm^{-1}.[30c] Symmetrical stretching bands of $-NH_3^+$ appear at around 2767, 2653, and 2528 cm^{-1}.[30c,44] The bands in the region of 2700−3100 cm^{-1} are assigned to the C−H stretching modes of the polymethylene ($-(CH_2)_n-$) chains (2852 cm^{-1}, $\nu_s(CH_2)$; 2923 cm^{-1}, $\nu_{as}(CH_2)$) and end-methyl ($-CH_3$) groups (2871 cm^{-1}, $\nu_s(CH_3)$; 2959 cm^{-1}, $\nu_{as}(CH_3)$).[45,46] A broad band appearing at around 2110 cm^{-1} is due to a combination of the asymmetrical bending vibration and torsional oscillation of the $-NH_3^+$ groups interacting with the apical oxygen of the W−O framework, i.e., $R-NH_3^+\cdots{}^-O-W$.[30c] When the XRD, TG results and CHN data are taken into account, it can therefore be concluded that the products obtained should be inorganic−organic hybrids with lamellar mesostructures, in which the inorganic W−O layers and the organic species (*n*-octylamine ions) are stacked alternately.

Other *n*-alkylamines with various alkyl chain lengths ($C_mH_{2m+1}NH_2$, $4 \le m \le 14$) were also used as guest molecules to react with $H_2W_2O_7 \cdot xH_2O$ in heptane. All the hybrids obtained exhibit strong (00l) reflections with sharp shapes in the low 2θ range in their XRD patterns (see the Supporting Information, Figure S4). This indicates that the inorganic−organic hybrids obtained are also of highly ordered lamellar structures. Their interlayer distances vary from 1.60(1) nm for $m = 4$ to 4.01(2) nm for $m = 14$. The number of obvious (00l) reflections increases from 3 to 10 as the *n*-alkyl-chain length increases from $m = 4$ to $m = 14$, indicating that the degree of the long-range order of the alternate inorganic−organic lamellar structure is enhanced by increasing the *n*-alkyl chain length of the *n*-alkylamine. SEM images (see the Supporting Information, Figure S5) show that all of those products obtained show belt/tubelike morphology, similar to the case of *n*-octylamine. TG analyses (see the Supporting Information, Figure S6) indicate that the tungstate-based inorganic−organic hybrids accommodating *n*-alkylamines with various *n*-alkyl chain lengths exhibit similar thermal decomposition processes judging from the similar TG curve profiles. The mass loss between room temperature and 873 K increases linearly with the *n*-alkyl chain length in *n*-alkylamine (from 46% for $m = 4$ to 71% for $m = 14$).

Structures of Tungstate-Based Inorganic−Organic Hybrids. The arrangement of the *n*-alkyl chains and the thickness of the inorganic layers can be evaluated by analyzing the variations in interlayer distance versus the alkyl chain length.[9b,11a,46−48] It is well-known that the relationship of the interlayer distance (d) to the carbon chain length (n_C) can generally be described as d (nm) $= d_0 + kn_C$, where k is the slope and d_0 is the intercept at $n_C = 0$, and that the increment per $-CH_2-$ for a fully extended all-trans alkyl chain is 0.127 nm.[5] The slope k can therefore give useful information about the arrangement of the *n*-alkyl chains. When $k \le 0.127$, the arrangement should be a monolayer with a tilt angle α ($\alpha = \sin^{-1}(k/0.127)$) or a bilayer with a smaller tilt angle.[5] When $0.127 < k \le 0.254$, a bilayered arrangement with a tilt angle of $\alpha = \sin^{-1}(k/0.254)$ is usually considered.[9c] The intercept d_0 corresponds to the sum of the thickness of the inorganic layer and the spatial separation due to the amine functional groups.

To investigate the development of the inorganic layers during the reactions, we prepared two extreme series of products, in the very early stage and in the completed stage, were prepared with $C_mH_{2m+1}NH_2$ ($4 \le m \le 14$) by employing reaction periods of 30 min and 5 days, respectively. The interlayer distances of the inorganic−organic hybrids obtained were determined by the (00l) reflections from XRD measurements. It should be noted that in the case of 30 min reaction time, another series of (00l) reflections, whose d values were similar to those of the corresponding hybrids

(43) Chernyshova, I. V.; Rao, K. H.; Vidyadhar, A.; Shchukarev, A. V. *Langmuir* **2000**, *16*, 8071.
(44) *Spectrometric Identification of Organic Compounds*; Silverstein, R. M., Basser, G. C., Morrill, T. C., Eds.; Willey: New York, 1991.
(45) Nuzzo, R. G.; Korenic, E. M.; Dubois, L. H. *J. Chem. Phys.* **1990**, *93*, 767.
(46) Park, S. H.; Lee, C. E. *Chem. Mater.* **2006**, *18*, 981.
(47) Matsumoto, A.; Odani, T.; Sada, K.; Miyata, M.; Tashiro, K. *Nature* **2000**, *405*, 328.
(48) Jaimez, E.; Slade, R. C. T. *J. Chem. Soc., Dalton Trans.* **1997**, 1435.

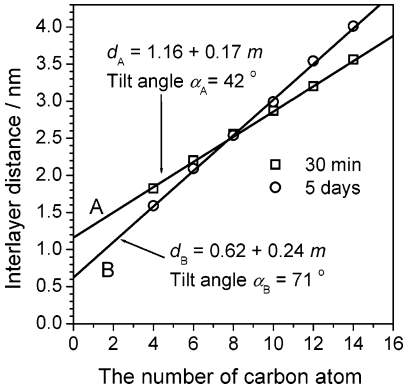

Figure 3. Plots of the interlayer distance (d) vs the number of carbon atoms in an *n*-alkyl chain (m, $C_mH_{2m+1}NH_2$) for (A) intermediates with a reaction time of 30 min and (B) hybrid nanotubes/nanobelts with a reaction time of 5 days.

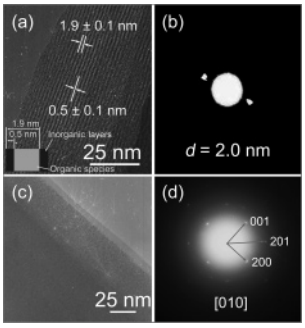

Figure 4. TEM observation of a tungstate-based inorganic−organic hybrid accommodating *n*-octylamine obtained in heptane with an *n*-octylamine: $H_2W_2O_7{\cdot}xH_2O$ molar ratio of 30: (a) a high-resolution TEM image and (b) an SAED pattern obtained with an incident electron beam parallel to the inorganic layers; (c) a high-magnification TEM image and (d) an SAED pattern obtained with an incident electron beam perpendicular to the inorganic layers.

with a 5 day reaction time, were superimposed in the XRD patterns of some products (m = 4, 6, 10). The interlayer distances, calculated from the series of (00l) reflections different from those of the corresponding hybrids with a 5 day reaction time, are therefore plotted versus the number of carbon atoms in *n*-alkylamine to determine the microstructure of the early stage intermediates (curve A in Figure 3). The result of the linear fit shows a perfect linear relationship: d_A (nm) = 1.16 + 0.17 m ($4 \le m \le 14$). The slope k_A is 0.17, and its intercept d_{0A} is 1.16 nm at m = 0. On the basis of the above analysis, the *n*-alkyl chains between the inorganic layers of the intermediates take on a bilayered arrangement with a tilt angle of $\alpha_A = 42°$, because $0.127 < k_A < 0.254$. The thickness of the inorganic layers can be estimated by extrapolating the interlayer distance for m = 1 (d_{1A} = 1.33 nm). Because the bond lengths of C−N and N−H in RNH_2 are 0.147 and 0.101 nm, respectively,[49] the length (l_1) of a CH_3NH_2 molecule or $CH_3NH_3^+$ ion can be estimated approximately as the sum (0.248 nm) of 0.147 and 0.101 nm. Due to the bilayered arrangement and the tilt angle ($\alpha_A = 42°$), the contribution of the organic layers (CH_3NH_2 molecules or $CH_3NH_3^+$ ions) to the interlayer distance (d_{1A}) can be estimated as $2l_1 \sin \alpha_A$ = 0.33 nm. The thickness of the inorganic layers can therefore be calculated by subtracting 0.33 nm from d_{1A}, i.e., 1.33 − 0.33 = 1.00 nm. On the other hand, the thickness of the double-octahedral W−O layers can be roughly estimated by $c/2$ = 0.93 nm, where c = 1.86(1) nm is the cell parameter of the $H_2W_2O_7$ without interlayer water.[38] It is clearly apparent that the value calculated from the intercept is very close to the thickness of the double-octahedral W−O layers, suggesting that the double-octahedral W−O layers are preserved in the intermediates obtained in an early stage.

To determine whether the double-octahedral W−O layers are retained in the final belt/tubelike nanostructures, we also give the plot of d versus m of the hybrids obtained after a reaction time of 5 days, as shown as curve B of Figure 3. There is also a perfect linear relationship between the interlayer distance and the number of carbon atoms in an *n*-alkyl chain: d_B (nm) = 0.62 + 0.24 m ($4 \le m \le 14$). Similarly, the slope coefficient of k_B = 0.24 suggests that the *n*-alkyl chains in the hybrids take on a bilayered arrangement with a tilt angle of $\alpha_B = \sin^{-1}(0.24/0.254) = 71°$. The thickness of the inorganic layers can be estimated according to a similar process: $d_{1B} - 2l_1 \sin \alpha_B = 0.86 - 0.47 = 0.39$ nm. It should be noted that this value (0.39 nm) is much lower than the thickness (0.931 nm) of the double-octahedral W−O layers, but very similar to the thickness (0.403 nm) of the single-octahedral W−O layers in H_2WO_4 or $H_2WO_4{\cdot}H_2O$.[30a]

Direct observation of the inorganic layers in the layered inorganic−organic hybrids using TEM is another reliable characterization technique. Carefully tuning the direction of the incident electron beams and choosing the proper observation spots can yield useful information about the thickness and the phase of the inorganic layers. Figure 4 shows a typical result for the inorganic−organic nanobelts accommodating *n*-octylamine with a reaction time of 5 days. Images a and b of Figure 4 show the high-resolution TEM image and the corresponding SAED pattern, respectively, of a case in which the incident electron beam is parallel to the inorganic layers. A black-to-white striped structure with a periodical range interval is observed in Figure 4a. The black stripes belong to inorganic layers and the white ones are organic species. The interlayer distance and the inorganic thickness can be estimated as 1.9 ± 0.1 nm and 0.5 ± 0.1 nm, respectively. The one-dimensional diffractional lattices shown in Figure 4b are typically characteristic of an ordered lamellar structure, the interlayer distance of which is about 2.0 nm calculated according to the equation $d = L\lambda/R$. The interlayer distance (2.0 nm) observed by TEM is slightly smaller than that obtained from the XRD results (about 2.5 nm), probably due to redispersing the hybrid in ethanol to make TEM samples.[19a] The directly observed thickness of the inorganic layer is much smaller than that of the double-octahedral W−O layers but close to the single-octahedral W−O layers.

The TEM image and its corresponding SAED pattern obtained with the incident electron beam perpendicular to the inorganic layers are shown in images c and d of Figure 4, respectively. The discernible two-dimensional diffractional lattices in the SAED pattern can be used to determine the phase of the inorganic layers. As Figure 4d shows, it can be

(49) *Lange's Handbook of Chemistry*; Dean, J. A., Ed.; McGraw-Hill: New York, 1999.

indexed to the $H_2WO_4 \cdot H_2O$ phase (JCPDS 18-1420) along the [010] zone axis. The result corroborates that the belt/tubelike hybrids consist of single-octahedral W−O layers and organic layers.

On the basis of discussion of the plots of interlayer distance versus carbon number of the *n*-alkyl chain and the TEM observation, it can be safely stated that the initial intermediates are intercalation compounds with double-octahedral W−O layers, which are then converted to be single-octahedral W−O layers during the continuing reaction. According to the mass losses and CHN data, as listed in Table 1, the molar ratios (*R*) of the amount of *n*-octylamine taken up to W in the inorganic layers are calculated for the products with various reaction periods, and the results are listed in Table 1. The *R* value increases from 0.563 to 2.16 when the reaction time increases from 0.5 to 120 h. It should be noted that there are two kinds of hybrids, one with double-octahedral W−O layers (in platelike particles) and another with single-octahedral layers (in belt/tubelike structures), respectively, in the intermediate reaction stages. The ratio of the amount of the hybrid with single-octahedral W−O layers to that of the hybrid with double-octahedral W−O layers increases with increases in reaction time, which accounts for the increase in the amount of *n*-alkylamine taken up. Supposing that the product with a 0.5 h reaction consists merely of plates and that the product obtained with a 120 h reaction consists merely of belts/tubes, the amounts of the platelike phase and the belt/tubelike phase in the products with various reaction periods of 1−25 h can roughly be estimated according to their *R* values. Given that the amounts of the belt/tubelike phase in the products with reaction periods of 0.5 and 120 h are 0 and 100%, respectively, on the basis of the amount of W atoms, the amounts for the belt/tubelike phase in the products with reaction periods of 1, 3, 5, 8, and 25 h are estimated to be about 2, 4, 26, 44, and 67%, respectively.

Formation Mechanism of Tungstate-Based Inorganic−Organic Hybrid Nanobelts/Nanotubes from $H_2W_2O_7 \cdot xH_2O$. On the basis of the analyses of morphological changes and microstructural development, the reaction behavior of $H_2W_2O_7 \cdot xH_2O$ with *n*-alkylamines can be schematically expressed using Figure 5. Figure 5a illustrates the possible pathway to the formation of belt/tubelike tungstate-based inorganic−organic hybrids. In the very early stages, the microscale $H_2W_2O_7 \cdot xH_2O$ particles are gradually cleaved into thin plates, which are aggregates of alternately stacked inorganic−organic layers with thicknesses of 200−800 nm (shown as A → B → C). With the continuation of the reaction, the thin plates are dissolved from their edges to form the final filamentous nanobelts, as shown in C → D. Some of the nanobelts with large widths are spontaneously scrolled into nanotubes to minimize the surface energy.

The microstructural development of the inorganic W−O layers and the arrangement of *n*-alkyl chains are illustrated in Figure 5b. The hydrophilic $H_2W_2O_7 \cdot xH_2O$ particles with interlayer water are first dispersed into the nonpolar heptane with the assistance of amphiphilic *n*-alkylamine molecules. The polar heads ($-NH_2$) of the *n*-alkylamines spread to the surfaces of the inorganic particles, and their alkyl tails spread toward the nonpolar continuous phase, as shown in E. In such reverse-micelle-like media with an excess of *n*-alkylamine, the *n*-alkylamine molecules can directionally diffuse from the nonpolar phase to the interlayer spaces of $H_2W_2O_7 \cdot xH_2O$ particles under the interactions of proton transfer. Consequently, normal intercalation occurs easily. The double-octahedral W−O layers are transitorily preserved in the early stage intermediates, constructed by alternately stacking the double-octahedral W−O layers and the bilayer-arranged *n*-alkylammonium ions with a small tilt angle. A typical microstructural model is shown as F. Upon intercalation of *n*-alkylamine, the interlayer water molecules are released to become "free" water, which then reacts with the surrounding *n*-alkylamine molecules to form highly alkaline solutions in the reverse-micelle-like media. In these space-confined highly alkaline solutions, the double-octahedral W−O layers are therefore dissolved from their edges, and the resultant species subsequently recrystallize to form highly ordered lamellar mesostructures with an alternate stacking of single-octahedral W−O layers and bilayer-arranged *n*-alkyl chain arrays with a large tilt angle, as shown in G. During the above course, the essential behavior of the

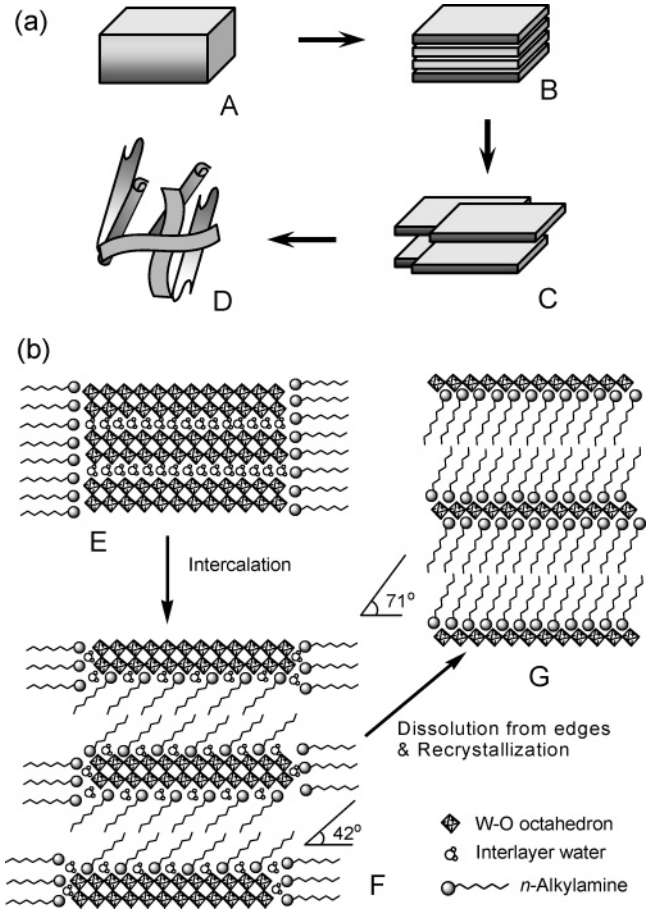

Figure 5. (a) Schematic diagram of the pathway to formation of belt/tubelike tungstate-based inorganic−organic nanostructures in a system of alkane/*n*-alkylamine/$H_2W_2O_7 \cdot xH_2O$. (b) A formation mechanism of tungstate-based inorganic−organic hybrids with single-octahedral W−O layers from layered $H_2W_2O_7 \cdot xH_2O$ particles with double-octahedral W−O layers.

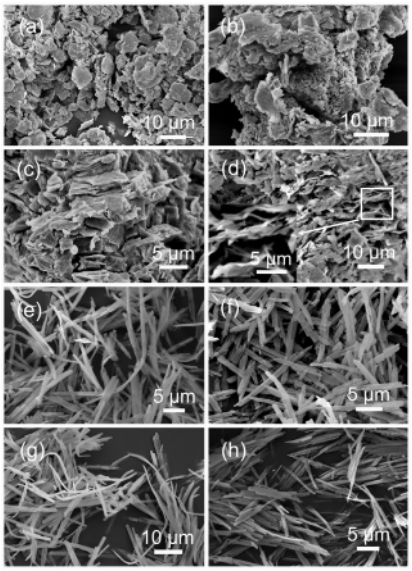

Figure 6. (a) SEM image of a hybrid obtained in heptane with an *n*-octylamine:$H_2W_2O_7{\cdot}xH_2O$ molar ratio of 2; (b−h) SEM images of hybrids obtained in various solvents with a molar *n*-octylamine-to-$H_2W_2O_7{\cdot}xH_2O$ ratio of 30: (b) ethanol, (c) THF, (d) 1-octanol, (e) pentane, (f) decane, (g) 2,2,4-trimethylpentane, and (h) cyclohexane.

reaction of $H_2W_2O_7{\cdot}xH_2O$ with *n*-alkylamine (RNH_2) can be expressed as follows

$$H_2W_2O_7{\cdot}xH_2O \xrightarrow{RNH_2} (RNH_3)_aH_{2-a}W_2O_7 + H_2O \quad (1)$$

$$RNH_2 + H_2O \rightarrow RNH_3^+ + OH^- \quad (2)$$

$$(RNH_3)_aH_{2-a}W_2O_7 \xrightarrow[RNH_2]{H_2O,\ OH^-} (RNH_3)_bH_{2-b}WO_4 \quad (3)$$

The initial molar ratios of *n*-octylamine to $H_2W_2O_7{\cdot}xH_2O$ in the reaction system have a remarkable effect on the morphology of the products. Figure 6a displays a typical SEM image of the product obtained after a reaction time of 5 days with a molar *n*-octylamine-to-$H_2W_2O_7{\cdot}xH_2O$ ratio of 2. Its major morphology is platelike particles with a diameter of about 10 μm, which differs distinctly from the belt/tubelike morphology of the hybrids obtained with high *n*-octylamine:$H_2W_2O_7{\cdot}xH_2O$ molar ratios (e.g., 30). The XRD pattern (see the Supporting Information, Figure S7) shows that the product obtained with a *n*-octylamine:$H_2W_2O_7{\cdot}xH_2O$ molar ratio of 2 also presents an ordered lamellar structure with an interlayer distance of $d = 2.56(2)$ nm, which is very close to that of the intermediate obtained after a 30 min reaction (molar *n*-octylamine:$H_2W_2O_7{\cdot}xH_2O = 30$, $d = 2.56(3)$ nm, curve A in Figure 3). This suggests that the microstructure of the hybrid obtained with a very low molar *n*-octylamine-to-$H_2W_2O_7{\cdot}xH_2O$ ratio is very similar to that of the intermediate obtained with a short reaction time. Its TG and CHN data are listed in Table 2, and the calculated molar ratio (R) of *n*-octylamine taken up to W is 0.738, which is close to the R value of the intermediate product with a 30 min reaction, but much smaller than that of the product obtained with an *n*-alkylamine-to-$H_2W_2O_7{\cdot}xH_2O$ ratio of 30 and a reaction time of 5 days (Table 1). The probable explanation is that the *n*-alkylamine molecules are barely sufficient for the reaction with $H_2W_2O_7{\cdot}xH_2O$ at a very low *n*-alkylamine:$H_2W_2O_7{\cdot}xH_2O$ molar ratio, and the interlayer water molecules released upon intercalation of *n*-alkylamine are most likely repulsed away from the hybrid particles formed. Thus the highly alkaline aqueous solutions cannot be formed. Without highly alkaline aqueous solutions, the double-octahedral W−O layers in platelike particles cannot be dissolved. As a result, the platelike morphology is retained. The morphological and microstructural change with the molar ratio of *n*-alkylamine to $H_2W_2O_7{\cdot}xH_2O$ strongly support the proposed mechanism.

The solvent types also have important influences on the reaction behavior of $H_2W_2O_7{\cdot}xH_2O$ with *n*-alkylamines. No reaction is observed, or the reactions occur to a very limited extent, in the solvents of 2-propanol, butanol, and acetone (XRD patterns in the Supporting Information, Figure S8). In the cases of ethanol and THF, no belt/tubelike shapes, but instead platelike ones are observed, as shown in images b and c of Figure 6, although the reactions proceed and the ordered lamellar mesostructures are obtained according to the XRD results (Figure S8). When 1-octanol is used as the reaction solvent, an ordered lamellar hybrid, with beltlike shapes besides a very small fraction of plates, is obtained (Figure 6d and the Supporting Information, Figure S8). With the solvents of nonpolar alkanes, on the other hand, including not only heptane but also other alkanes, such as pentane, decane, 2,2,4-trimethylpentane, and cyclohexane, inorganic−organic hybrids with uniform belt/tubelike morphology are readily obtained, as shown in Figure 6e−h. Their XRD patterns (see the Supporting Information, Figure S8) indicate that all these products obtained with other alkanes possess highly ordered lamellar mesostructures.

It should be noted that only one path to formation of the hybrid nanobelt/nanotubes with single-octahedral W−O layers exists; the formation of intercalation compounds, the dissolution of the intercalation compounds and subsequent recrystallization of the dissolved species are sequential

Table 2. Summary of Mass Loss (M_L) between Room Temperature and 873 K, Data for CHN Analysis, the Molar Ratio (R) of *n*-Octylamine Taken up to W, and Morphology of the Products Obtained in Various Systems through a Reaction of $H_2W_2O_7{\cdot}xH_2O$ with *n*-Octylamine for 5 Days

reaction system							
solvent	*n*-octylamine/ $H_2W_2O_7{\cdot}xH_2O$	M_L (mass %)	C (mass %)	H (mass %)	N (mass %)	R	morphology
heptane	2:1	30.5	21.24	4.47	3.10	0.738	plates
ethanol	30:1	35.3	24.24	5.18	3.57	0.913	plates
THF	30:1	35.9	24.12	5.14	3.56	0.919	plates
1-octanol	30:1	50.3	35.01	7.15	4.33	1.44	belts
pentane	30:1	52.5	38.10	7.94	5.60	1.95	belts/tubes
decane	30:1	52.6	38.13	7.97	5.51	1.92	belts/tubes
2,2,4-trimethylpentane	30:1	59.1	40.57	8.13	5.57	2.25	belts/tubes
cyclohexane	30:1	52.8	44.48	8.65	6.05	2.12	belts/tubes

events, and the release of water from the interlayer spaces of $H_2W_2O_7 \cdot xH_2O$ is the key step. The effect of the solvents on the morphology of the products is therefore mainly due to their ability to exclude the released interlayer water, which reacts with excess *n*-alkylamine to form the highly alkaline aqueous solutions. As long as the highly alkaline aqueous solutions are formed, the subsequent belt/tubelike hybrids with single-octahedral W−O layers can be readily achieved by dissolving the initial intercalation compounds and recrystallizing the dissolved species. In the systems of *n*-alkylamine/$H_2W_2O_7 \cdot xH_2O$/ethanol and *n*-alkylamine/$H_2W_2O_7 \cdot xH_2O$/THF, the solvents of ethanol and THF are miscible with H_2O. The interlayer water molecules released upon intercalation of *n*-alkylamine can easily diffuse into the solvents. Under these circumstances, highly alkaline aqueous solutions cannot be formed. As a result, dissolution of the double-octahedral W−O layers of the intercalation compounds and subsequent recrystallization do not occur in the H_2O-miscible solvents. This may well account for the fact that the platelike morphology is retained in ethanol and THF. On the contrary, 1-octanol is immiscible with H_2O and the *n*-octylamine/$H_2W_2O_7 \cdot xH_2O$/1-octanol system can behave like an *n*-octylamine/$H_2W_2O_7 \cdot xH_2O$/alkane system.[50] Highly alkaline aqueous solutions, confined by the reverse-micelle-like media, can therefore be formed in the *n*-octylamine/$H_2W_2O_7 \cdot xH_2O$/1-octanol system, in which dissolution and recrystallization are subsequently able to occur.

The mass losses, CHN data and the calculated molar ratios (R) of the amount of *n*-octylamine taken up to W in the inorganic layers are summarized in Table 2. On the basis of Figure 6 and Table 2, the morphology of the products in various solvents seems to correlate with the amount of *n*-alkylamine taken up. The products with low R values take on a platelike morphology, whereas those with high R values exhibit belt/tubelike shapes. The ratios for the belt/tubelike hybrids are almost twice as large as those for the hybrids with platelike morphologies (Table 2). These phenomena strongly support the conclusion that the platelike products possess double-octahedral W−O layers, which are then dissolved and recrystallized to form belt/tubelike hybrids with single-octahedral W−O layers. All these results are highly consistent with the proposed mechanism.

(50) (a) Gradzielski, M.; Hoffmann, H.; Panitz, J.-C.; Workaun, A. *J. Colloid Interface Sci.* **1995**, *169*, 103. (b) Poole, S. K.; Poole, C. F. *J. Chromatogr., B* **2003**, *797*, 3. (c) Koetz, J.; Bahnemann, J.; Kosmella, S. *J. Polym. Sci., Part A: Polym. Chem.* **2004**, *42*, 742.

Conclusions

We have systematically investigated the behavior of reactions between layered $H_2W_2O_7 \cdot xH_2O$ and *n*-alkylamines ($C_mH_{2m+1}NH_2$, $4 \leq m \leq 14$) under ambient conditions. Tungstate-based inorganic−organic hybrid nanobelts/nanotubes with highly ordered lamellar mesostructures and tunable interlayer distances (from 1.60 to 4.01 nm) have been synthesized in nonpolar solvents with high *n*-alkylamine:$H_2W_2O_7 \cdot xH_2O$ molar ratios (e.g., 30). During the formation of tungstate-based belt/tubelike hybrids, the platelike intercalation compounds with double-octahedral W−O layers are formed in the very initial stages, accompanying the release of interlayer water molecules upon intercalation of *n*-alkylamine. The double-octahedral W−O layers of the initially formed intercalation compounds are then dissolved from their edges in the highly alkaline aqueous solutions, which are derived from the hydrolysis of excess *n*-alkylamine in the released interlayer water confined by the reverse-micelle-like media. The dissolved species finally recrystallize to form belt/tubelike hybrids with single-octahedral W−O layers.

Acknowledgment. This work was supported by the 21st Century COE Program, "Practical NanoChemistry", of the Ministry of Education, Culture, Sports, Science and Technology, Japan, and by Waseda University as a special research project (2005B-161).

Supporting Information Available: A typical TEM image of an as-prepared inorganic−organic hybrid in heptane with an *n*-octylamine:$H_2W_2O_7 \cdot xH_2O$ molar ratio of about 30; TG curves of hybrids accommodating *n*-octylamine obtained after various reaction times in the solvent of heptane (*n*-octylamine:$H_2W_2O_7 \cdot xH_2O$ molar ratio of about 30); FT−IR spectra of inorganic−organic hybrids accommodating *n*-alkylamine ($C_mH_{2m+1}NH_2$, $m = 4, 8, 12$); the XRD patterns, SEM images, and TG curves of the products accommodating *n*-alkylamines with various *n*-alkyl chain lengths ($m = 4, 6, 8, 10, 12, 14$); the XRD pattern of a product obtained after a reaction time of 5 days in heptane with an *n*-octylamine:$H_2W_2O_7 \cdot xH_2O$ molar ratio of 2, and the XRD patterns of products obtained after a reaction time of 5 days in various solvents (*n*-octylamine:$H_2W_2O_7 \cdot xH_2O$ molar ratio of 30). This material is available free of charge via the Internet at http://pubs.acs.org.

CM062039U